Mechanics of Materials 71 (2014) 62–73

Contents lists available at ScienceDirect

Mechanics of Materials

journal homepage: www.elsevier.com/locate/mechmat

Dislocation reactions, plastic anisotropy and forest strengthening in MgO at high temperature

J. Amodeo [a,*], B. Devincre [b], Ph. Carrez [a], P. Cordier [a]

[a] Unité Matériaux et Transformations, UMR CNRS 8207, Université de Lille 1, Cité Scientifique, 59655 Villeneuve d'Ascq, France
[b] Laboratoire d'Etude des Microstructures, UMR 104, CNRS-ONERA, 29 avenue de la Division Leclerc, 92322 Chatillon, France

ARTICLE INFO

Article history:
Received 6 November 2013
Received in revised form 21 December 2013
Available online 18 January 2014

Keywords:
MgO
Plasticity
Dislocation Dynamics simulation
Forest strengthening

ABSTRACT

The collective properties of dislocations in MgO are investigated in the high temperature regime and at constant strain rate with 3D Dislocation Dynamics simulations. Intersections between slip systems 1/2⟨110⟩{110} and 1/2⟨110⟩{100} allow essentially two types of junction reactions. These junctions are energetically stable and are expected to promote strong forest strengthening at high temperature. Large-scale DD simulations show that MgO strain hardening at high temperature may be dominated by forest reactions. Important parameters for dislocation density based modeling of MgO plasticity are finally calculated and verified to be consistent with experimental observations.

1. Introduction

MgO is a model ceramic with NaCl-structure intensively studied in the past decades for its potential uses as a refractory material (T_f > 3000 K at ambient pressure). Alloyed to a small amount of iron (~10%), MgO is also the second most abundant phase of the Earth's lower mantle after the magnesium-silicate perovskite phase $MgSiO_3$. Therefore, the study of MgO plastic properties is of great interest in both Geophysics and Materials Sciences.

At ambient pressure, plastic strain in MgO single crystal is expected to be governed either by lattice friction, impurities strengthening or dislocation–dislocation elastic interactions depending on the investigated temperature range (Barthel, 1984; Haasen et al., 1985; Sato and Sumino, 1980).

At low temperature, a large lattice friction is measured on the two experimentally observed slip systems 1/2⟨110⟩{110} and 1/2⟨110⟩{100}, respectively. Dislocations in the 1/2⟨110⟩{110} slip system are found to glide at the lowest stress level (Barthel, 1984). In both slip systems, the kink-pairs nucleation process is the glide controlling rate mechanism and plastic deformation is governed by the slow motion of long screw dislocations (Appel and Wielke, 1985). At intermediate temperatures, lattice friction is less important and dislocations interactions with solute elements start to affect the MgO flow stress (Appel et al., 1984; Gorum et al., 1960; Srinivasan and Stoebe, 1974). The MgO mechanical properties in this intermediate temperature regime was recently overviewed by Messerschmidt (2010). Lastly, at temperatures higher than the athermal transition temperature T_a (respectively about 600 K and 1500 K for the 1/2⟨110⟩{110} and the 1/2⟨110⟩{100} slip systems), new features are expected to influence MgO plastic properties. Deformation microstructures are now made of curved dislocation segments and small debris (Clauer and Wilcox, 1976; Haasen et al., 1986). Whatever the active slip system and the impurity concentration, MgO flow stress is low about 10 MPa in this temperature regime (Amodeo et al., 2011; Copley and Pask, 1965; Hulse et al., 1963).

Very few quantitative analysis exist on the elementary mechanisms controlling MgO plasticity in the high

* Corresponding author. Present address: INSA Lyon, Laboratoire MATEIS, UMR CNRS 5510, 25 avenue Jean Capelle, 69621 Villeurbanne Cedex, France. Tel.: +33 472 438235; fax: +33 472 438539.
E-mail address: jonathan.amodeo@insa-lyon.fr (J. Amodeo).

http://dx.doi.org/10.1016/j.mechmat.2014.01.001
0167-6636/

temperature regime (Copley and Pask, 1965; Day and Stokes, 1964). This matter of fact is problematic as MgO has gained in recent years renewed interest to investigate small scale plasticity (Dong et al., 2010; Gaillard et al., 2006; Howie et al., 2012; Korte and Clegg, 2011; Korte et al., 2011) and in geophysics (Amodeo et al., 2012; Cordier et al., 2012; Girard et al., 2012; Merkel et al., 2002). For instance, Cordier and collaborators (2012) have recently shown that the mechanical properties of MgO in the athermal regime (*i.e.* for $T > T_a$) are of primary importance to understand the rheology of the Earth's lower mantle. For these reasons, it is expected that Dislocation Dynamics (DD) simulations dedicated to MgO plasticity can provide new inputs and hopefully can improve our understanding of the Earth's mantle flow mechanisms.

Three-dimensional DD simulations are today acknowledged as a unique tool to investigate collective properties of dislocations and to access crystal plasticity at the microstructure level (*i.e.* at the mesoscopic scale). DD simulations have shown interest in lots of different studies, but mainly in the case of metal plasticity (Bulatov et al., 2006; Devincre et al., 2008; Dimiduk et al., 2006; Madec et al., 2003). In a recent study, it was shown that MgO yield stress can be precisely evaluated with DD simulations for MgO single crystals and large grains polycrystals (Amodeo et al., 2011). Here, we present new calculations performed in the athermal regime to examine the contribution of forest reactions to MgO plastic flow at ambient pressure and in laboratory conditions of strain rate.

The effect of forest interactions (*i.e.* dislocation–dislocation contact reactions) is explored in two steps. First, we systematically investigate the reactions occurring between two intersecting dislocations depending on their slip systems and their relative orientations. Then, large-scale DD simulations are performed to quantify the contribution of forest interactions to plastic strain depending on the active slip systems. Finally, we calculate physical parameters, which are essential ingredients of crystal plasticity models at large scale.

2. Simulations methodology

2.1. Dislocation Dynamics simulations

Dislocation Dynamics simulations have been performed with the free and open source simulation code *microMegas* (mM). Full description of this computer model has been presented in numerous studies (see for example, Devincre et al., 2001; Durinck et al., 2007; Monnet et al., 2004), and was recently described with some details in Devincre et al. (2011). More specific information on the local rules applied in the simulation to model junction zipping-unzipping can be found in Carrez et al. (2005), Devincre (1996), and Devincre et al. (2006). In the following, we recall some basics and calculation specificities of the present work.

The mM simulation relies on a discretization of both space and time. For each slip systems, dislocation lines are discretized into a set of straight segments with discrete character including screw, edge and mixed directions. Those segments move on a 3D cubic lattice with glide directions here reproducing the symmetry of MgO crystal lattice. Forces on dislocation segments are calculated using standard formula taken from the dislocation elastic theory (Devincre and Condat, 1992; Hirth and Lothe, 1982). The effective resolved shear stress calculated at the center of dislocation segments takes into account the internal stress field associated with the whole set of dislocation lines present in the simulated volume, the applied stress accounting for the loading conditions and a line tension correction term accounting for the elastic energy lost when replacing locally curved dislocation sections by straight segments. Local rules are prescribed in the simulation to account for contact interactions, such as annihilations or the locking of sessile dislocation junctions in specific crystallographic directions. For the present study, the length of the Burgers vector $1/2\langle 1\,1\,0\rangle$ for dislocations in MgO is set to 2.99 Å and isotropic elasticity is used with a shear modulus $\mu(T) = 140 - 0.0255 * T$ (Isaak et al., 1989, 1990; Karki et al., 2000) and a constant Poisson ratio $\nu = 0.18$.

2.2. Dislocation intersection mapping

The first simulations reported in Section 3 are dedicated to the mapping of dislocation–dislocation intersections. This type of simulations depicts possible reactions between two intersecting dislocations and provides preliminary information on the strength of forest interactions between slip systems. Such type of calculations have already been made in several materials including FCC and BCC structures (Kubin et al., 2003; Madec et al., 2002a; Madec and Kubin, 2004; Wickham et al., 1999), HCP structures (Capolungo, 2011; Monnet et al., 2004) and other materials like olivine (Durinck et al., 2007) and ice (Devincre, 2012). Carrez and collaborators also published a first numerical investigation of the dislocation interactions between $1/2\langle 1\,1\,0\rangle\{1\,1\,0\}$ slip systems in MgO (Carrez et al., 2005).

The methodology to calculate a map of dislocation–dislocation intersections with DD simulations is now standard and proceeds as follows. Two straight dislocations segments, crossing at their centers, are introduced in a large simulation cell and relaxed by considering only dislocation glide. Depending on the initial configuration, different kind of reactions can be observed like junction, annihilation, crossed or repulsive states. These simulations are completely driven by elastic energy minimization and no applied stress is imposed. The tested configurations are defined by the two angles (φ_1, φ_2) existing in between the initial segments directions and the intersection between their glide planes (Fig. 1).

2.3. Massive DD simulations

The second set of simulations reported in Section 3 aims at reproducing the collective properties of dislocations in the athermal regime during compression tests at constant strain rate (referred as massive DD simulation in the following). As we want to simulate plastic deformation for $T > T_a$, use is made of a free flight mobility law:

$$v(\tau) = \frac{b\tau}{B} \tag{1}$$

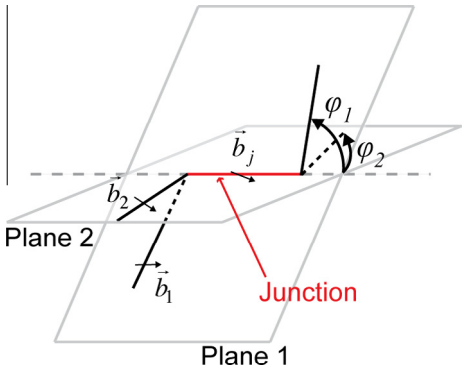

Fig. 1. Two parent dislocation lines, with Burgers vectors $\vec{b}_1$ and $\vec{b}_2$, interact each other leading to the formation of a dislocation junction with Burgers vector $\vec{b}_j = \vec{b}_1 + \vec{b}_2$. The nature of the two parent dislocations is defined by the angles (φ_1, φ_2).

This mobility law is supposed to be dislocation character and slip plane independent. The viscous drag coefficient B accounts for dissipating processes and refers to the atomistic mechanisms that control dislocation mobility at high temperature in ionic crystals (*i.e.* phonon drag and interactions between charged dislocations and their compensating charged clouds). Without any reliable value of B in MgO (Kardashev et al., 1985) a common value measured in ionic crystals of $B = 10^{-5}$ Pa s is considered (Robinson, 1972; Singh et al., 2008). Results of DD simulations are not expected to depend on the details of this free flight mobility law in materials with forest strengthening.

In massive DD simulations, a random distribution of edge and screw Frank–Read (F–R) sources with a density ρ is taken as initial dislocation microstructure. The length of sources, $l = 10\,\rho^{-1/2}$, is set large enough to avoid the simulated flow stress to be controlled by critical stress for dislocation multiplication at sources. As we will focus here on forest strengthening, the dislocation cross-slip and climb mechanisms were not taken into account in the simulations. Dislocation self-annihilation is a possible artifact of DD simulations when using periodic boundary conditions (Bulatov et al., 2000; Madec et al., 2004; Queyreau, 2008). Among the different existing solutions for this problem, a rotation of the crystal directions with respect to the $\langle 100 \rangle$ surfaces of periodicity and the use of a non-cubic shape for the simulation cell are used in the present work. Hence, whatever the investigated slip systems, the simulated crystal is rotated three times around different $\langle 111 \rangle$ directions in the simulation cell frame. This operation corresponds to the rotation matrix reproduced in Table 1.

Because DD simulation does not allow for large strains and therefore for large increase of the dislocation density, simulations starting with different initial dislocation densities must be performed to test forest strengthening at different virtual level of strain (Madec et al., 2002b). For this reason, we used a scaling method that provides different dislocation densities from a reference simulation by scaling all the characteristic lengths of the investigated problem with a unique factor. Here, considering a reference simulation volume V_{ref}, the dislocation density is defined

Table 1
The rotations matrix applied to the MgO crystal in the simulation frame to control periodic boundaries artifacts.

$$\begin{bmatrix} \bar{1} & \bar{4} & 8 \\ 4 & 7 & 4 \\ \bar{8} & 4 & 1 \end{bmatrix}$$

by $\rho_{ref} = N_{ref} * l_{ref}/V_{ref}$. N_{ref} and l_{ref} refer respectively to the number of F–R sources and their length. Then, an alternative simulation will be parameterized by a scaling factor f that impose an initial dislocation density:

$$\rho = \rho_{ref} \left(f_{ref}/f\right)^2 \tag{2}$$

Outcomes of this scaling method and other key parameters used in the massive DD simulations are summarized in Table 3.

3. Results

3.1. Mapping of dislocation–dislocation intersections

3.1.1. Preliminary analysis

In MgO and usually in materials with the NaCl crystalline structure, plastic deformation is known to take place in the two $1/2\langle 110 \rangle\{110\}$ and $1/2\langle 110 \rangle\{100\}$ slip system families. Each family is made of 6 independent slip systems noted hereafter with index i as listed in Table 2.

Geometrical examination and Frank's rule for dislocation reactions (Friedel, 1967) give preliminary elements of analysis on the possible dislocation reactions that may exist between slip systems. Considering all slip systems noted in Table 2, 66 combinations of dislocation interaction exist (*i.e.* 15 per slip system family plus 36 reported as "crossed" configurations between $1/2\langle 110 \rangle\{110\}$ and $1/2\langle 110 \rangle\{100\}$ slip systems). Accounting for the MgO crystal symmetries, those 66 combinations can be grouped in 7 different classes of intersections (*i.e.* 2 per slip system family and 3 for the "crossed" configurations). Within such classes, 1 type per slip system family corresponds to coplanar or orthogonal intersections. Such reactions have very low probability and are not energetically favorable. Therefore, they are not expected to strongly contribute to forest strengthening. For this reason, they will not be detailed further in the present study. Readers interested in such intersections may refer to Carrez et al. (2005) for more details. Then, one remains only with:

Table 2
Indexation of the 12 MgO slip systems considered in the present work.

$1/2\langle 110 \rangle\{110\}$			$1/2\langle 110 \rangle\{100\}$		
i	Plane	$\vec{b}$	i	Plane	$\vec{b}$
1	$(\bar{1}10)$	$\frac{1}{2}[110]$	7	(001)	$\frac{1}{2}[110]$
2	(110)	$\frac{1}{2}[1\bar{1}0]$	8	(001)	$\frac{1}{2}[1\bar{1}0]$
3	$(0\bar{1}1)$	$\frac{1}{2}[011]$	9	(100)	$\frac{1}{2}[011]$
4	(011)	$\frac{1}{2}[01\bar{1}]$	10	(100)	$\frac{1}{2}[101]$
5	$(\bar{1}01)$	$\frac{1}{2}[101]$	11	(010)	$\frac{1}{2}[101]$
6	(101)	$\frac{1}{2}[10\bar{1}]$	12	(010)	$\frac{1}{2}[10\bar{1}]$

- One type of intersections between $1/2\langle 1\,1\,0\rangle\{1\,1\,0\}$ slip systems:

This type of intersections (intersection between slip systems $i = 2$ and 4 for instance) corresponds to contact interactions between dislocations in slip systems with Burgers vectors oriented at 60° or 120° each other (Copley and Pask, 1965; Kear et al., 1959). In this case, the expected junction is of edge character, directed along the $\langle 1\,1\,1\rangle$ directions, with a $1/2\langle 1\,1\,0\rangle$Burgers vector. Its potential glide plane is {112}, which is not an identified glide plane in MgO. For this reason, such junction was considered as sessile in the simulations. This reaction is called the 60°/120°{110} junction in the following.

- One type of intersections between $1/2\langle 1\,1\,0\rangle\{1\,0\,0\}$ slip systems:

This orthogonal intersecting slip systems configuration (systems $i = 8$ and 9 for instance) can form $1/2\langle 1\,1\,0\rangle\{1\,1\,0\}$ edge junctions along the $\langle 1\,0\,0\rangle$ directions. It is later mentioned as the 90°{100} junction.

- Three types of "crossed" intersections between $1/2\langle 1\,1\,0\rangle\{1\,1\,0\}$ and $1/2\langle 1\,1\,0\rangle\{1\,0\,0\}$ slip systems:
  (i) Intersections involving slip systems with the same Burgers vectors (systems $i = 1$ and 7 for instance) are specials. They correspond to the particular case of collinear annihilations. Collinear annihilation is the reaction promoting the strongest of all possible forest strengthening. In the last years, the exceptional properties of this reaction was the matter of several investigations (Devincre et al., 2005; Madec et al., 2003).
  (ii) Intersections between slip systems with 90° Burgers vectors (slip systems $i = 1$ and 8 for instance) may form junctions with mixed character, potentially glissile in the {100} planes. Nevertheless, the $\langle 1\,0\,0\rangle$ Burgers vector of such junctions is too large to be energetically favorable and this intersection only leads to repulsive and crossed-states.
  (iii) Intersections between slip systems with 60°/120° Burgers vectors (slip systems $i = 3$ and 12 for instance) can form mixed junctions with Burgers vector $1/2\langle 1\,1\,0\rangle$. Those junctions are glissile in the {100} planes.

3.1.2. Dislocation intersection maps in MgO

DD simulation is a powerful numerical tool to quantify the domains of reactions occurrence in the above listed intersections. The intersection maps reported in Fig. 2 are based on interaction simulations between dislocation segments with length $l = 1$ μm intersecting at the center of a cubic simulation cell with 3 μm linear dimension. To calculate these maps, 676 (φ_1, φ_2) initial configurations are systematically tested to explore a wide range of possible intersection configurations (we test 26 different segment characters for each slip systems). Following the work of Madec et al. (2002b), the simulation results are systematically compared to the predictions of a simple elastic model (Hirth and Lothe, 1982) neglecting the contribution of dislocation curvature to the relaxation problem. It must be noted that for all the configurations we tested in the case of MgO, a good match is found between the DD simulation results and the predictions of this simple elastic model.

Fig. 2a and b shows respectively the results of 60°/120°{110} and the 90°{100} intersection maps. In these maps, the junction domains are well delimited with round shapes. In such lobes, the junction length (and consequently the junction strength) is decreasing rapidly when approaching the domain frontiers. The junction domains represent in both maps approximately 40% of the intersections and the remaining relaxed configurations are repulsive interactions or crossed-states, both in similar proportions.

Fig. 2c and d refer to "crossed" intersections *i.e.* involving slip systems from the two MgO slip system families. For sake of brevity, only "crossed" configurations leading to energetically favorable reactions are represented. The intersection map inferred from "crossed" slip systems with Burgers vectors oriented at 60°/120° each other (Fig. 2c), *e.g.* $1/2[0\,1\,1](0\,\bar{1}\,1)$ and $1/2[1\,0\,\bar{1}](0\,1\,0)$, is characterized by a junction domain larger than those observed in the 60°/120°{110} and 90°{100} intersections. Like in other materials, the collinear interaction map (Fig. 2d) shows that the annihilation domains are much larger than the attractive regions calculated with conventional elastic predictions (68% of favorable geometrical configurations). Hence, collinear annihilation is potentially a very efficient forest strengthening mechanism if slip system activities allow for its occurrence.

These intersection map results are interesting and show that, in agreement with the forest model (Saada, 1960), strong dislocation line "pinning" induced by junction reactions and collinear annihilations take place in MgO plastic deformation if the temperature is large enough to facilitate dislocation mobility. While intersection map calculations allow identifying dislocation–dislocation reaction types, they strictly do not quantify forest strengthening. This is why, more complex DD simulations, accounting for the collective properties of dislocations are now presented.

3.2. Massive DD simulations

Numerical straining experiments at constant strain rate have been performed to study plastic deformation and forest strengthening in MgO. As the literature always relates mechanical tests where dislocations glide either in the $1/2\langle 1\,1\,0\rangle\{1\,1\,0\}$ slip system family or in the $1/2\langle 1\,1\,0\rangle\{1\,0\,0\}$ slip system family (Appel et al., 1984; Copley and Pask, 1965; Day and Stokes, 1964), we restricted simulations to symmetric multi-slip conditions with initial dislocation densities including only one set of slip system family. In these simulations, the initial dislocation density ρ_{init} is equally distributed between each of the six possible slip systems per family.

First, compression tests with the $1/2\langle 1\,1\,0\rangle\{1\,1\,0\}$ slip systems were made using a $\langle 1\,0\,0\rangle$ loading axis. This orientation allows to activate dislocation glide in four of the six possible slip planes with a Schmid factor $S = 0.5$. In those simulations, the MgO shear modulus was set to

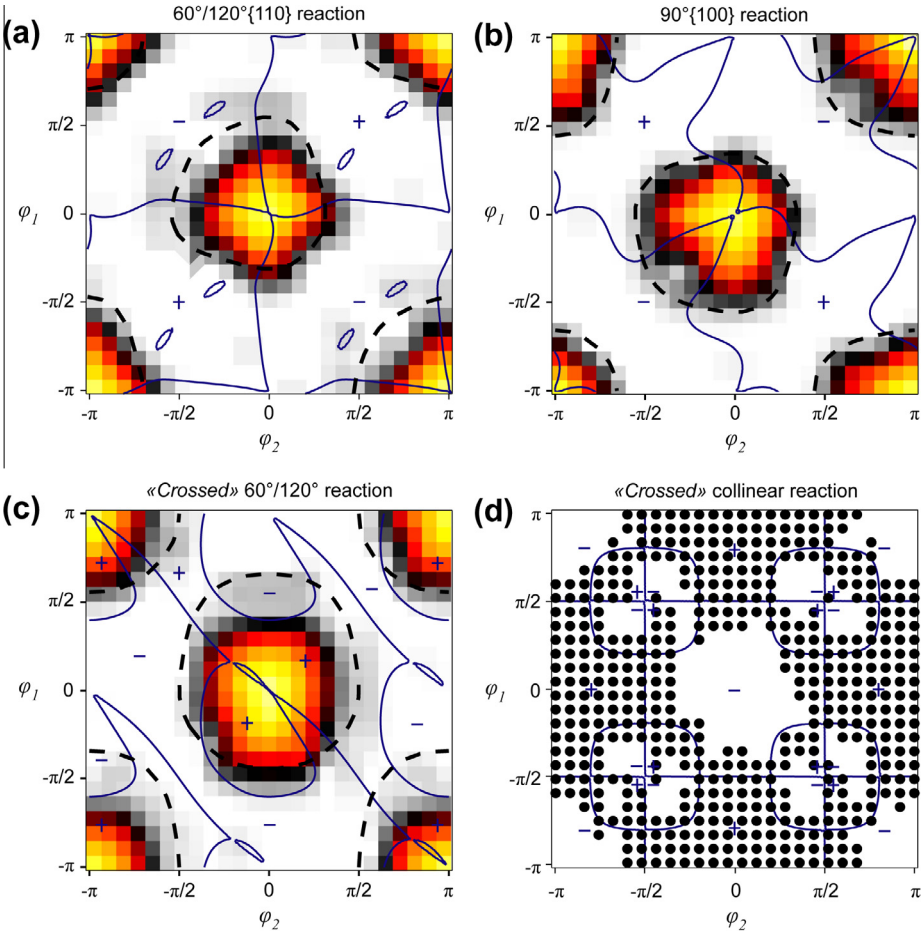

Fig. 2. Dislocation intersection maps (a) the 60°/120°{1 1 0} reaction, (b) the 90°{1 0 0} reaction, (c) the "crossed" 60°/120° reaction and (d) the "crossed" collinear reaction. Solid lines delimit repulsive (−) and attractive (+) domains and dashed lines refer to junction lobes calculated with a simple elastic model. (a)–(c) Each figure pixel represents a (φ_1,φ_2) initial configuration leading to a junction in the simulation. Colors refer to the junction length l_j (from light gray for shortest junctions up to yellow for largest junctions). In the middle of the junction lobe, (0,0), the dislocation segments are parallel to the junction direction, hence $l_j = l$. (d) Black solid circles refer to geometrical configurations favorable to annihilations. (For interpretation of the references to color in this figure legend, the reader is referred to the web version of this article.).

114.5 GPa to reflect a temperature equal to 1000 K. It must be noted that such temperature is significantly above the $1/2\langle 1\,1\,0\rangle\{1\,1\,0\}$ slip system athermal temperature which is approximately equal to 600 K. The reference dislocation density and simulated volume are respectively $\rho_{ref} = 10^{12}$ m^{-2} and $V_{ref} = 10.70 \times 11.70 \times 11.80\ \mu m^3$.

A second set of calculations was carried out with the $1/2\langle 1\,1\,0\rangle\{1\,0\,0\}$ slip system family. To compare with experimental observations such simulations have been made using a shear modulus of 89 GPa consistent with a temperature of 2000 K. Again, it must be noted that such temperature is above the tested slip systems athermal temperature which is approximately equal to 1500 K. The loading axis is along the $\langle 1\,1\,0\rangle$ directions. Four of six $1/2\langle 1\,1\,0\rangle\{1\,0\,0\}$ slip systems are thus activated with a Schmid factor $\sqrt{2}/4$ ($\sim$0.35). The reference dislocation density is still $\rho_{ref} = 10^{12}\ m^{-2}$, but the dimensions of the simulation reference volume was modified to account for different dislocation self-annihilation directions, $V_{ref} = 8.00 \times 9.09 \times 10.32\ \mu m^3$.

3.2.1. Strain rate calibration

In DD simulations, considering a dislocation viscous mobility law like Eq. (1), one may define two deformation regimes respectively at low and high strain rate (Kubin et al., 1998). At low strain rate, the simulated flow stress is mostly insensitive to strain rate variations if the dislocation dynamics is governed by forest interactions. This low strain rate case is called "quasi-static" regime and suits to the mechanical behavior of FCC metals in laboratory tests, typically in the range of $10^{-4}\ s^{-1}$ up to $1\ s^{-1}$. Rising the strain rate, DD simulation switches to the "dynamic" regime. In this high strain rate regime, a large density of immobile dislocations pinned at forest obstacles do not anymore rule plastic strain, but rather the latter is controlled by dislocations velocity during their free flight. Contrary to the "static" regime, the "dynamic" regime is then strongly sensitive to strain rate.

In order to verify that our simulations refer to conventional "quasi-static" conditions (flow stress independent of strain rate), three increasing strain rates were

investigated: 1 s^{-1}, 10 s^{-1} and 100 s^{-1}. These simulations are made considering the 1/2⟨1 1 0⟩{1 1 0} reference setup described above.

The shear stress τ versus plastic shear γ_p curves we get with these simulations are presented in Fig. 3a. Similar results are found at 1 s^{-1} and 10 s^{-1} strain rate and the dislocation dynamics observed are found very closed in the simulated volume. Discrepancies start to appear only at 100 s^{-1} with a slight increase of the flow stress. It must be noted that similar behavior was observed with the simulations considering the 1/2⟨1 1 0⟩{1 0 0} slip systems. The slopes of the simulated plastic deformation versus time plotted with a linear regression are respectively 0.98 s^{-1}, 9.96 s^{-1} and 99.40 s^{-1} (Fig. 3b). These values are in good agreement with the imposed strain rate meaning that the strain rate regime is achieved whatever the simulation conditions.

From the above remarks and considering a dislocation density $\rho_{ref} = 10^{12}$ m^{-2}, DD simulations show that MgO single crystal deforms within the "static" regime below 10 s^{-1} imposed strain rate. Between 10 s^{-1} and 100 s^{-1}, simulations enter the "dynamic" regime. In this regime, the calculated flow stress is questionable since it is controlled by dislocation mobility equation which is poorly known in the MgO at high temperature. Nevertheless, it is interesting to note that the transition range we reproduced between the two regimes is close to the one calculated in previous simulations made in FCC and BCC crystals (Devincre and Kubin, 1997; Kubin et al., 1998; Madec, 2001; Queyreau, 2008). This result suggests that the strength of forest interactions in MgO at high temperatures is closed to those found in FCC and BCC metals.

3.2.2. Dislocation avalanches and plastic anisotropy

Simulations made at the reference density ($\rho_{ref} = 10^{12}$ m^{-2}) show that the flow stress is about 10 MPa for the both 1/2⟨1 1 0⟩{1 1 0} and 1/2⟨1 1 0⟩{1 0 0} slip systems families. During these simulations, the dislocation microstructure evolves through the formation and destruction of lots of junctions, which impose a jerky motion to mobile dislocations. As for FCC metals (Devincre et al., 2008), the athermal deformation regime of MgO is thus characterized by the discontinuous motion of dislocations, through consecutive long waiting periods and few glide events sometime called "dislocation avalanches". This non-linear dynamics justify the use of DD simulations to do up-scaling and to identify parameters for continuum models.

To illustrate dislocation avalanches in MgO, we superimposed eight successive views taken from a thin foil of 1 μm, oriented along the [$\bar{1}$ 1 0] direction (Fig. 4). From this setup, one can follows the jerky glide of a 1/2[1 1 0]($\bar{1}$ 1 0) dislocation passing through the whole thin foil (from positions marked 1–8). After entering the thin foil (bottom of Fig. 4, position 1), the dislocation alternates gliding and pinned configurations due to the formation and the destruction of junctions. This mechanism is especially well depicted at positions 3 and 4 where junctions are clearly identified as pinning obstacles to dislocation glide. The dislocation is finally stopped in position 8, where two strong junctions and a dipole finish to impede its progression. It must be noted in Fig. 4 that only the progression of one dislocation is reproduced, but during large plastic burst, the simulated dislocation avalanches involve several mobile dislocations in parallel glide planes.

In accordance with Section 3, numerous 60°/120°{1 1 0} and 90°{1 0 0} junctions, oriented along the ⟨1 1 1⟩ and the ⟨1 0 0⟩ directions can be observed in the simulated dislocation microstructures (Fig. 5). Whatever the activated slip system, both dislocation and junction densities (respectively ρ and ρ_j) increase during deformation, whereas the ratio ρ_j/ρ quickly saturates in between 30% and 40% as already observed in FCC similar investigations (Devincre et al., 2008).

Furthermore, we note that during simulations, the density of junctions per slip system $\rho_{j,i}$ does not increase homogeneously with strain. Such tendency is observed even for slip systems stressed with the same Schmid factor. Furthermore, this phenomenon is found in all simulations whatever the tested slip system families or the initial dislocation density. For the sake of brevity, only the case of the 1/2⟨1 1 0⟩{1 1 0} reference simulation is analyzed in the following.

Fig. 6b illustrates the different evolution of the $\rho_{j,i}$ distribution calculated for each activated (i = 1 to 4) and inactive slip systems (i = 5 and i = 6) in the early stages of the 1/2⟨1 1 0⟩{1 1 0} with the reference density. From deformation as small as $\varepsilon_p \sim 0{,}04\%$, it is clear that in the large periodic volume element used in massive DD simulation, a strong deviation of the number of junctions is detected on mechanically equivalent slip systems. This unbalanced

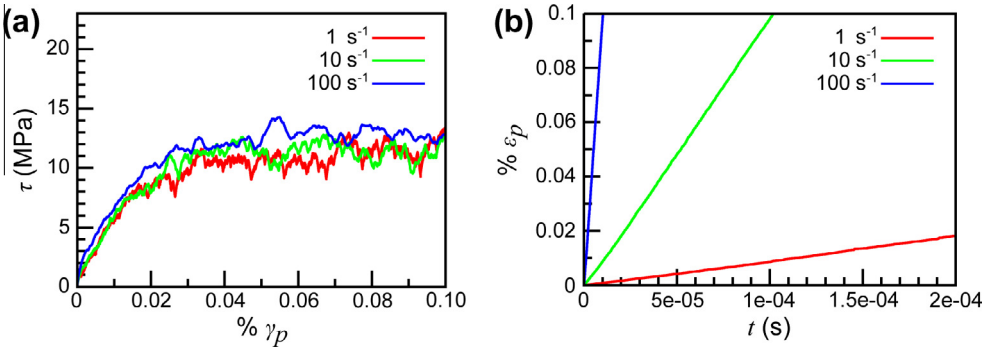

Fig. 3. Shear stress τ versus plastic shear γ_p (a) and plastic deformation ε_p versus time t (b) for strain rates of 1 s^{-1}, 10 s^{-1} and 100 s^{-1}.

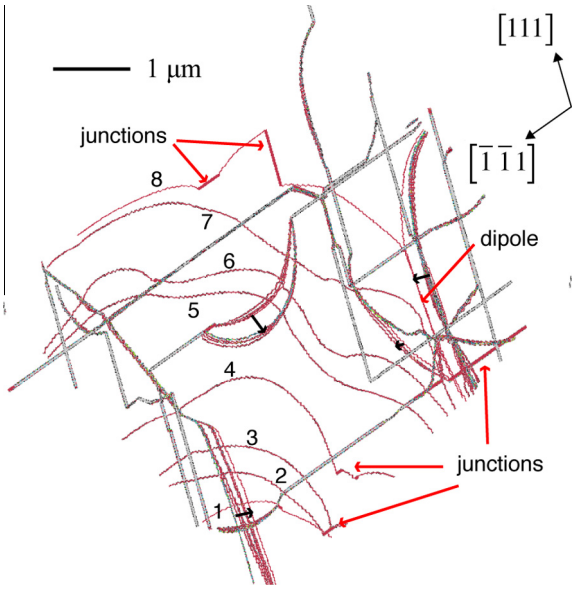

Fig. 4. 8 successive views of a thin foil of 1 μm thick, oriented along the [1 $\bar{1}$ 0] direction, are superimposed. Static dislocation lines are represented in gray and gliding dislocation segments in red. Numbers 1–8 refer to successive positions of the dislocation involved within a plastic burst (avalanche). Black arrows point out small displacements (bow out) of neighboring dislocations. (For interpretation of the references to color in this figure legend, the reader is referred to the web version of this article.).

evolution is not load controlled, but is rather ruled by heterogeneities in the microstructure formed during the deformation. Using different initial dislocation source distribution allows checking this point. Indeed, it is found that a tiny heterogeneity in the initial dislocation distribution quickly promotes unbalanced formation of junctions between active slip systems. Such differences help or restrict the mobility of dislocations and affect the multiplication rate of dislocation in the slip systems (Fig. 6a). The larger is the dislocation density on a given slip system (for instance slip system $i = 1$ in Fig 6), the more such system acts as forest obstacles to the other slip systems and decreases the density of mobile dislocations. This is why, as for $\rho_{j,i}$, the plastic shear distribution between slip system $\gamma_{p,i}$ is also anisotropic (Fig. 6a) and the total plastic strain is governed at the end of simulations by the activity of one or few dominating slip systems (*e.g.* $i = 1$ and 2 in Fig. 6).

3.2.3. Forest strengthening in MgO

The simulations of reference reported in the previous sections with both 1/2⟨1 1 0⟩{1 1 0} and 1/2⟨1 1 0⟩{1 0 0} slip system families highlight the important role of dislocation–dislocation contact interactions in the athermal deformation regime. In metals, the forest model (Saada, 1960) is the most pertinent model accounting for the influence of dislocation microstructure on the plastic flow. This model justifies the well-known Taylor form:

$$\tau_f = \alpha \mu b \sqrt{\rho} \tag{3}$$

where α is a temperature independent coefficient which averages the effect of all possible dislocation–dislocation interactions, ρ_f is the forest dislocation density (*i.e.* the density of dislocations cutting to the glide plane of mobile dislocations) and τ_f the athermal stress required to overcome the forest dislocations network.

However, Eq. (3)refers only to a simplified expression of the dislocation line tension which neglects small variations associated to a logarithmic term in the definition of the dislocation elastic energy (Hirth and Lothe, 1982). Both experiments and simulations have proved this logarithmic contribution to be significant (*i.e.* systematic deviations from Eq. (3)are observed), especially for large values of ρ_f. This is why, alternative forms of the Taylor equation which account for the exact energetics of dislocation line tension exist. For instance, Devincre et al. (2006) proposed a modified forest expression with the form:

$$\tau_f = \mu b \frac{ln\left(1/b\sqrt{\beta\rho_f}\right)}{ln\left(1/b\sqrt{\beta\rho_{ref}}\right)}\sqrt{\beta\rho_f} \tag{4}$$

where β is a forest strengthening coefficient equivalent to α , but which does not depend on the dislocation density.

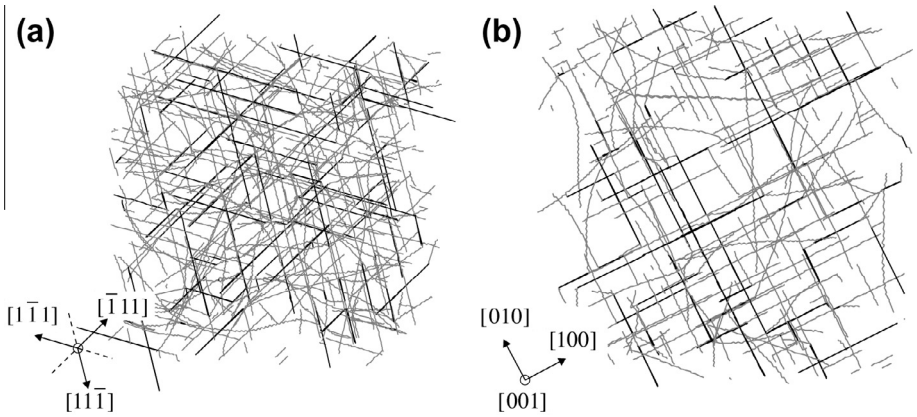

Fig. 5. Two example of dislocation microstructure for simulations with the 1/2⟨1 1 0⟩{1 1 0} slip system (a) and the 1/2⟨1 1 0⟩{1 0 0} slip system (b). Dislocations are represented in gray and junctions are in black.

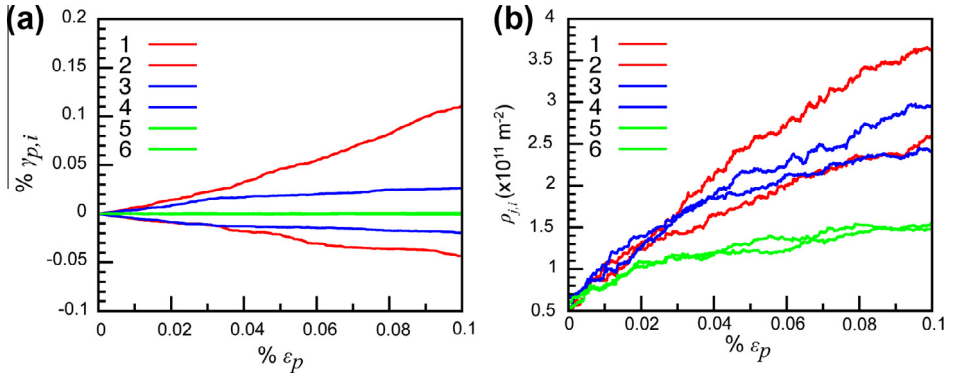

Fig. 6. Plastic shear per slip system $\gamma_{p,i}$ (a) and evolution of the junction density per slip system $\rho_{j,i}$ (b) during simulations with the $1/2\langle 110\rangle\{110\}$ slip system family and the reference density. In the legend, numbers refer to the slip system index presented Table 1. Curves with identical colors refer to orthogonal slip systems. (For interpretation of the references to color in this figure legend, the reader is referred to the web version of this article.).

In order to see if the forest model also applies for MgO single crystal deformation in the athermal regime, simulations using the scaling method described in Section 2 were performed. This scaling methodology allows crossing a broad range of dislocation densities without increasing CPU costs. Details on the key parameters used for these calculations are summarized in Table 3.

Here, we define the effective forest density ρ_f as the glide planes intersecting dislocation density, what leads to $\rho_f = 5/6\rho$ and $\rho_f = 2/3\rho$ respectively for simulations in $\{110\}$ and $\{100\}$ slip planes. In the case of $\{100\}$, the dislocation density attributed to coplanar slip systems is subtracted. As expected, the stress–strain curves presented in Fig. 7 show that the larger the dislocation density, the higher the flow stress. As an effect of the plastic instability discussed above, plastic deformation is progressively localized in one or two "easy" slip system. This explains why dislocation dynamics is modified from multi-slip to easy slip conditions and why a smooth softening effect is observed at the end of the stress–strain curves (Fig. 7). To quantify the influence of each slip system on forest strengthening, this plastic anisotropy phenomenon must be handled carefully. The forest coefficients α and β were therefore calculated using the following protocol: (i) stress and dislocation density measurements are performed after yield, but after relatively low simulated plastic deformations and before the occurrence of plastic anisotropy (ii) the imposed strain rate regime must be achieved.

Table 3
Key parameters of the massive DD simulations made at different scales. The same parameters are applied for simulations with slip systems $1/2\langle 110\rangle\{110\}$ and $1/2\langle 110\rangle\{100\}$. f, ρ_{init}, V, dt, $\dot{\varepsilon}$ and Φ are respectively the simulation scaling factor, the initial dislocation density, the simulation cell volume, the time step, the imposed strain rate and the dislocation discretization length. The parameters used for the reference simulations are noted in bold.

f	ρ_{init} (m^{-2})	V (μm^3)	dt ($\times 10^{-10}$ s)	$\dot{\varepsilon}$ (s^{-1})	Φ (μm)
31.6	1×10^{11}	~31600	2	1	0.63
10	$\mathbf{1 \times 10^{12}}$	**~1000**	**0.66**	**10**	**0.20**
4.47	5×10^{12}	~89	0.30	50	0.09
3.16	1×10^{13}	~32	0.066	100	0.06

Evolution of the resolved shear stress on active slip systems regarding the square root of the forest density is plotted in Fig. 8. These results are compared with predictions of Eqs. (3) and (4) in order to fit, the α and β coefficients values. From this plot we see that the standard Taylor equation (Eq. (3)) fits well DD simulation results with α values of 0.24 when considering the $1/2\langle 110\rangle\{110\}$ slips and 0.28 with the $1/2\langle 110\rangle\{100\}$ slips. Comparison with Eq. (4)gives even a better agreement and leads to β values of 0.07 and 0.10 (using a reference dislocation density of 10^{12} m^{-2}) for the $1/2\langle 110\rangle\{110\}$ and $1/2\langle 110\rangle\{100\}$ slip system families respectively (see Fig. 8). As expected, the main benefit of Eq. (4) appears at the extreme values of the forest density.

The close correspondence between the α (or β) forest coefficients found with the two tested slip system families confirms statistically the first predictions made with the dislocations intersection maps. The dislocation reactions taking place during the $1/2\langle 110\rangle\{110\}$ and $1/2\langle 110\rangle\{100\}$ slip systems simulations, *i.e.* mainly the 60°/120°$\{110\}$ and the 90°$\{100\}$ junctions, have comparable stability and therefore impose close forest strengthening. Finally, the low level of plastic deformation simulated with DD simulations and the softening instability observed in the MgO simulations make direct comparison to experiment a difficult exercise. One can only say that forest interaction, which is the only strengthening mechanism considered in the present study, reproduce realistic flow stress for MgO plasticity in the athermal regime.

4. Discussion

4.1. Comparison to experiments and other DD simulations studies

Intersections between slip planes in high temperature compression tests with MgO single crystal have been mentioned very early, especially for the $\{110\}$ slip planes (Copley and Pask, 1965; Day and Stokes, 1964; Groves and Kelly, 1963). In compression tests, it was shown that MgO deforms with $1/2\langle 110\rangle\{110\}$ slips thanks to the activation of only one or few glide directions whereas other

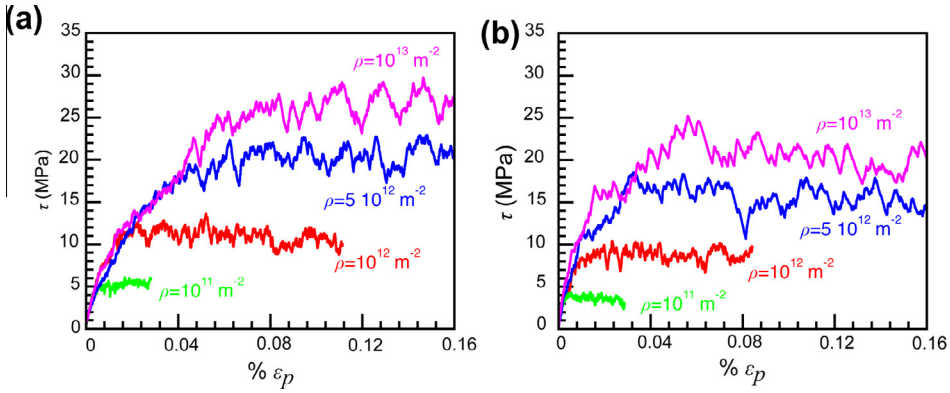

Fig. 7. Stress–strain curves for simulations with the 1/2⟨110⟩{110} slip systems (a) and the 1/2⟨110⟩{100} slip systems (b).

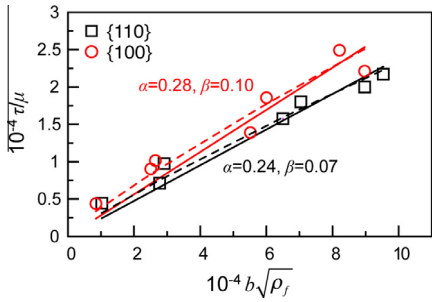

Fig. 8. Simulated flow stress evolution as function of forest density for the two MgO slip system families. Symbols represent DD simulation results. Straight and dashed lines correspond to the least-squares resolution of Eqs. (3) and (4), respectively.

observed slip systems seem to be blocked. Qualitative interpretation of such plastic anisotropy is today based on the assumption that strong interactions exist between slip systems.

In this work, two different approaches based on the dislocation elastic theory and making use of DD simulations (dislocation intersection mapping and large-scale massive simulation) were used.

First, the intersection maps presented in Section 3 lead to the definition of several different interaction geometries which support the formation of strong junctions when dislocations intersect between two different slip systems. The 60°/120°{110} and the 90°{100} intersection maps exhibit comparable statistics of junction occurrence with 40% of favorable configurations (Fig. 2a and b). Both intersection maps are highly comparable to the well-known Lomer-Cottrell reaction observed in FCC crystals (Madec et al., 2002a). This similitude comes partly from the direction 1/2⟨110⟩ and the amplitude of the existing dislocation Burgers vector in MgO that is closed to the FCC case. In addition, it was shown that the dimensions of the junction domains obtained in all MgO intersection maps are larger than the Hirth junction solution existing in FCC crystals (Kubin et al., 2003; Wickham et al., 1999) and also is larger or equivalent to most junction solutions found in BCC crystals (Kubin et al., 2003; Wickham et al., 1999). Hence, forest strengthening in MgO is expected to be large in the absence of strong lattice friction and comparable to FCC and BCC metals results. In addition, we found that numerous collinear annihilations can occur in MgO plastic deformation if the two 1/2⟨110⟩{110} and 1/2⟨110⟩{100} slip system families are simultaneously activated. This possibility could induce very large forest strengthening.

Secondly, massive DD simulations have been performed to quantitatively determine forest strengthening in MgO. Experimental observations (Washburn et al., 1960) of an increase of the dislocation density in the four ⟨111⟩ directions when only the 1/2⟨110⟩{110} slip systems are activated is well reproduced with the DD simulations. This observation is simply explained by the formation of ⟨111⟩ sessile 60°/120°{110} junctions that block dislocation glide in these directions.

The formation of MgO dislocation microstructures in multi-slip conditions involves the accumulation of many junctions and is found to systematically promote plastic anisotropy. This "autocatalytic" phenomena, justified in Section 3, may explain frequent macroscopic observations made in MgO deformation experiments (Copley and Pask, 1965; Day and Stokes, 1964; Hulse and Pask, 1960).

The increase of flow stress with the increase of dislocation density found in massive simulations follows Taylor's types relations (Eqs. (3)and (4)) and validates the existence of a strong forest strengthening in MgO at high temperature. The calculated Taylor coefficient α is 0.24 and 0.28 with the 1/2⟨110⟩{110} and 1/2⟨110⟩{100} slip system families respectively. Such values agree with experimental measurements of about 0.2 (Davidge and Pratt, 1964). However, too few measurements of α have been performed in MgO to make a strong statement. In addition, calculation of the β coefficients is made. The latter coefficient is important as it provide information for ceramic micromechanical models at much lower and higher dislocation density than considered in DD simulations.

Taylor coefficients (α or β) compare well for the two slip system families observed in MgO. This result is easily understood by the similarity of dislocation microstructures, in terms of junction's strength and probability of occurrence. While the 60°/120°{110} junction in MgO and the FCC Lomer–Cottrell junctions lead to similar domain of existence in intersection maps, the value of α for the 1/2⟨110⟩{110} slip systems of MgO is lower than the

0.30–0.35 values measured (or calculated) in aluminum, copper or silver (Basinski and Basinski, 1979; Hansen and Huang, 1998). Such difference can be explained by (i) a lack of collinear annihilations, in MgO conventional strain conditions, which is considered to be an important ingredient of forest strengthening in FCC metals (Madec et al., 2003), (ii) a higher number of slip systems per family in FCC (12 instead of 6 in MgO) that increase the number of slip systems reaction causing the formation of junctions.

4.2. Toward a description of the strain hardening rate

Several deformation experiments in MgO report measurements about strain hardening rate coefficient $\theta = d\tau/d\gamma$ in temperature ranges comparable to the one tested in the present simulations (Copley and Pask, 1965; Hulse and Pask, 1960; Routbort, 1979). Unfortunately, as for the flow stress question, there is today no strong argumentation on the physical process controlling hardening in MgO.

Following the seminal work of Kocks and Mecking (Kocks and Mecking, 2003; Mecking and Kocks, 1981), one can define a simple relation which links α to θ based on the derivative of Eq. (3) with respect to plastic strain :

$$\theta = \frac{(\alpha\mu b)^2}{2\tau}\frac{d\rho_f}{d\gamma} \tag{5}$$

Here, no attempt has been made to formally calculate the dislocation storage rate $d\rho_f/d\gamma$ existing in the second part of Eq. (5). This quantity results from a complex competition between different storage and recovery mechanisms, which are poorly known in MgO at high temperature. Rather, we made only a rough evaluation of this quantity directly from the DD simulations assuming that plastic anisotropy is not problematic when dislocation storage is averaged on several active slip systems. Hence, we estimated $d\rho_f/d\gamma$ about 2.09 $10^{14}\,m^{-2}$ and 4.15 $10^{14}\,m^{-2}$ from reference simulations in the $1/2\langle 1\,1\,0\rangle\{1\,1\,0\}$ and the $1/2\langle 1\,1\,0\rangle\{1\,0\,0\}$ slip system family, respectively. With these evaluations and the previously calculated values of α, work hardening rate evaluations are reported in Fig. 9.

These calculated values of θ are about $\mu/250$ at 1000 K for $1/2\langle 1\,1\,0\rangle\{1\,1\,0\}$ and of $\mu/130$ at 2000 K for $1/2\langle 1\,1\,0\rangle\{1\,0\,0\}$. Such strain hardening coefficients are larger than reported experimentally (Copley and Pask, 1965; Hulse and Pask, 1960; Routbort, 1979). Possible explanation for such over-evaluation may be that the simulated dislocation storage rates are necessarily overestimated in the absence of dislocation recovery mechanism. Indeed, θ is experimentally measured at large deformation, where recovery mechanisms are efficient (Routbort, 1979). Nevertheless, it is interesting to note that DD simulations give the right order of magnitude for θ without any fitting procedure. This matter of fact reinforces the idea of a prominent role of forest interactions on MgO plastic deformation in the athermal regime.

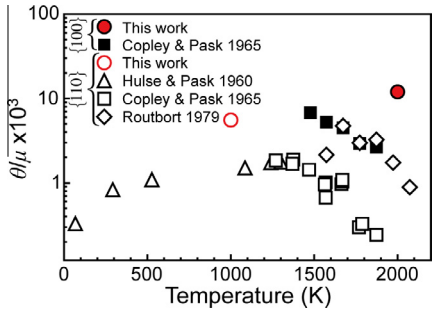

Fig. 9. Calculations (red symbols) of the strain hardening rate coefficient θ are compared to experimental data (black symbols) for both slip systems families $1/2\langle 1\,1\,0\rangle\{1\,1\,0\}$ and $1/2\langle 1\,1\,0\rangle\{1\,0\,0\}$. (For interpretation of the references to color in this figure legend, the reader is referred to the web version of this article.).

5. Conclusion

The main goal of this work was to identify possible existing reactions between dislocations in MgO and to quantify their influence on plastic flow at high temperature. Intersection maps calculations emphasize the importance of two energetically favorable junction reactions, *i.e.* the 60°/120°$\{1\,1\,0\}$ and the 90°$\{1\,0\,0\}$ junctions. These junctions act as strong pinning point in dislocation microstructures and justify strong forest strengthening and hardening in large-scale massive DD simulations of MgO at high temperature.

While this study gives a better understanding of the elementary mechanisms responsible for MgO plastic properties at high temperature, we also believe that the present results qualitatively apply for other materials with same crystallographic geometry like alkali halides (NaCl, KCl, LiF, etc.) where similar plastic behavior was observed experimentally (Takeuchi et al., 2009).

The present results are important for Materials Science where MgO plays a significant role as a model ceramic. In addition, MgO plasticity investigations are of primary importance for Earth Sciences considering the abundance of this phase in the lower mantle.

Here we show that $1/2\langle 1\,1\,0\rangle\{1\,1\,0\}$ and $1/2\langle 1\,1\,0\rangle\{1\,0\,0\}$ slip systems strengthen in similar proportions (α of 0.24 and 0.28, respectively) at ambient pressure and in the athermal regime of deformation. This result differs strongly from MgO mechanical behavior below T_a, where MgO deforms at stresses one order of magnitude lower in $1/2\langle 1\,1\,0\rangle\{1\,1\,0\}$ than in $1/2\langle 1\,1\,0\rangle\{1\,0\,0\}$. Based on a multiscale modeling approach, Cordier and collaborators (2012) have recently shown that in the Earth's conditions of pressure, temperature and strain rate, MgO deforms mainly in the athermal regime (Cordier et al., 2012). Nevertheless, their description of MgO plasticity was limited to the early stage of deformation. In calculating forest-strengthening coefficients for MgO at high temperature, the present study provides new important inputs regarding MgO strain hardening properties. To explore larger deformation properties and afford more advanced information on the mantle rheology, the development of physically justified crystal plasticity models is of primary importance. In this context, the question of MgO strain hardening properties under the Earth's conditions of pressure, temperature and strain rate is an upcoming challenge.

Acknowledgements

The authors are grateful to L.P. Kubin and R. Madec for helpful discussions. B. Devincre acknowledges the support of the M-ERA.net project FASS. Ph. Carrez acknowledges the support of the French ANR program (ANR Project DIUP). P. Cordier is supported by funding from the European Research Council under the Seventh Framework Programme (FP7), ERC Grant N 290424 – RheoMan.

References

Amodeo, J., Carrez, P., Cordier, P., 2012. Modelling the effect of pressure on the critical shear stress of MgO single crystals. Philos. Mag. 92, 1523–1541.

Amodeo, J., Carrez, P., Devincre, B., Cordier, P., 2011. Multiscale modelling of MgO plasticity. Acta Mater. 59, 2291–2301.

Appel, F., Bartsch, M., Messerschmidt, U., Nadgornyi, E., Valkovskii, S., 1984. Dislocation motion and plasticity in MgO single crystals. Phys. Status Solidi A 83, 179–194.

Appel, F., Wielke, B., 1985. Low temperature deformation of impure MgO single crystals. Mater. Sci. Eng. 73, 97–103.

Barthel, C., 1984. Plastiche Anisotropie von Bleisulfid und Magnesiumoxid (Diploma thesis). University of Gottingen.

Basinski, S., Basinski, Z., 1979. Plastic deformation and work hardening. In: Nabarro, F., Hirth, J. (Eds.), Dislocations in Solids. North-Holland, Amsterdam, pp. 261–362.

Bulatov, V., Hsiung, L., Tang, M., Arsenlis, A., Bartelt, M., Cai, W., Florando, J., Hiratani, M., Rhee, M., Hommes, G., 2006. Dislocation multi-junctions and strain hardening. Nature 440, 1174–1178.

Bulatov, V., Rhee, M., Cai, W., 2000. Periodic boundary conditions for dislocation dynamics simulations in three dimensions. In: Kubin, L., Selinger, R., Bassani, J., Cho, K. (Eds.), Multiscale Modeling of Materials, Symposium Proceedings. Materials Research Society, Warrendale, PA, pp. z1–z3.

Capolungo, L., 2011. Dislocation junction formation and strength in magnesium. Acta Mater. 59, 2909–2917.

Carrez, P., Cordier, P., Devincre, B., Kubin, L., 2005. Dislocation reactions and junctions in MgO. Mater. Sci. Eng. A 400, 325–328.

Clauer, A., Wilcox, B., 1976. High temperature tensile creep of magnesium oxide single crystals. J. Am. Ceram. Soc. 59, 89–96.

Copley, S., Pask, J., 1965. Plastic deformation of MgO single crystals up to 1600 C. J. Am. Ceram. Soc. 48, 139–146.

Cordier, P., Amodeo, J., Carrez, P., 2012. Modelling the rheology of MgO under Earth's mantle pressure, temperature and strain rates. Nature 481, 177–180.

Davidge, R., Pratt, P., 1964. Plastic deformation and work hardening in NaCl. Phys. Status Solidi B 6, 759–776.

Day, R., Stokes, R., 1964. Mechanical behavior of magnesium oxide at high temperatures. J. Am. Ceram. Soc. 47, 493–503.

Devincre, B., 1996. Meso-scale simulation of the dislocation dynamics. In: NATO ASI Series E Applied Sciences–Advanced Study Institute, vol. 308, pp. 309–324.

Devincre, B., 2012. Dislocation dynamics simulations of slip systems interactions and forest strengthening in ice single crystal. Philos. Mag. 93, 235–246.

Devincre, B., Condat, M., 1992. Model validation of a 3D simulation of dislocation dynamics: discretization and line tension effects. Acta Metall. Mater. 40, 2629–2637.

Devincre, B., Hoc, T., Kubin, L., 2005. Collinear interactions of dislocations and slip systems. Mater. Sci. Eng. A 400, 182–185.

Devincre, B., Hoc, T., Kubin, L., 2008. Dislocation mean free paths and strain hardening of crystals. Science 320, 1745–1748.

Devincre, B., Kubin, L., 1997. The modelling of dislocation dynamics: elastic behaviour versus core properties. Philos. Trans. R. Soc. A: Math. Phys. Eng. Sci. 355, 2003–2012.

Devincre, B., Kubin, L., Hoc, T., 2006. Physical analyses of crystal plasticity by DD simulations. Scr. Mater. 54, 741–746.

Devincre, B., Kubin, L., Lemarchand, C., Madec, R., 2001. Mesoscopic simulations of plastic deformation. Mater. Sci. Eng. A 309, 211–219.

Devincre, B., Madec, R., Monnet, G., Queyreau, S., Gatti, R., Kubin, L., 2011. Mechanics of Nano-Objects. Presse de l'Ecole des Mines de Paris, Modeling crystal plasticity with dislocation dynamics simulations the microMegas code.

Dimiduk, D., Woodward, C., LeSar, R., Uchic, M., 2006. Scale-free intermittent flow in crystal plasticity. Science 312, 1188–1190.

Dong, Z., Huang, H., Kang, R., 2010. An investigation of the onset of elastoplastic deformation during nanoindentation in MgO single crystal (001) and (110) planes. Mater. Sci. Eng. A 527, 4177–4184.

Durinck, J., Devincre, B., Kubin, L., Cordier, P., 2007. Modeling the plastic deformation of olivine by dislocation dynamics simulations. Am. Mineral. 92, 1346.

Friedel, J., 1967. Dislocations. Pergamon Press, Oxford.

Gaillard, Y., Tromas, C., Woirgard, J., 2006. Quantitative analysis of dislocation pile-ups nucleated during nanoindentation in MgO. Acta Mater. 54, 1409–1417.

Girard, J., Chen, J., Raterron, P., 2012. Deformation of periclase single crystals at high pressure and temperature: quantification of the effect of pressure on slip-system activities. J. Appl. Phys. 111, 112607–112607–5.

Gorum, A., Luhman, W., Pask, J., 1960. Effect of impurities and heat-treatment on ductility of MgO. J. Am. Ceram. Soc. 43, 241–245.

Groves, G.W., Kelly, A., 1963. The dislocation distribution in plastically deformed magnesium oxide. Proc. R. Soc. A: Math. Phys. Eng. Sci. 275, 233–244.

Haasen, P., Barthel, C., Suzuki, T., 1985. Choice of slip system and peierls stresses in the NaCl structure. In: Suzuki, H., Ninomiya, T., Sumino, K., Takeuchi, S. (Eds.), Dislocations in Solids. University of Tokyo Press, Tokyo, pp. 455–462.

Haasen, P., Messerschmidt, U., Skrotzki, W., 1986. Low energy dislocation structures in ionic crystals and semiconductors. Mater. Sci. Eng. A 81, 493–507.

Hansen, N., Huang, X., 1998. Microstructure and flow stress of polycrystals and single crystals. Acta Mater. 46, 1827–1836.

Hirth, J.P., Lothe, J., 1982. Theory of Dislocations. Wiley, New York.

Howie, P., Korte, S., Clegg, W., 2012. Fracture modes in micropillar compression of brittle crystals. J. Mater. Res. 27, 141–151.

Hulse, C., Copley, S., Pask, J., 1963. Effect of crystal orientation on plastic deformation of magnesium oxide. J. Am. Ceram. Soc. 46, 317–323.

Hulse, C., Pask, J., 1960. Mechanical properties of magnesia single crystals corn pression. J. Am. Ceram. Soc. 43, 373–378.

Isaak, D., Anderson, O., Goto, T., 1989. Measured elastic moduli of single-crystal MgO up to 1800 K. Phys. Chem. Miner. 16, 704–713.

Isaak, D., Cohen, R., Mehl, M., 1990. Calculated elastic and thermal properties of MgO at high pressures and temperatures. J. Geophys. Res. 95, 7055–7067.

Kardashev, B., Kustov, S., Lebedev, A., Berezhkova, G., Perstnev, P., Appel, F., Messerschmidt, U., 1985. Acoustic and electron microscopy study of the dislocation structure in MgO crystals. Phys. Status Solidi A 91, 79–87.

Karki, B., Wentzcovitch, R., De Gironcoli, S., Baroni, S., 2000. High-pressure lattice dynamics and thermoelasticity of MgO. Phys. Rev. B 61, 8793–8800.

Kear, B., Taylor, A., Pratt, P., 1959. Some dislocation interactions in simple ionic crystals. Philos. Mag. 4, 665–680.

Kocks, U., Mecking, H., 2003. Physics and phenomenology of strain hardening: the FCC case. Prog. Mater. Sci. 48, 171–273.

Korte, S., Clegg, W., 2011. Discussion of the dependence of the effect of size on the yield stress in hard materials studied by microcompression of MgO. Philos. Mag. 91, 1150–1162.

Korte, S., Ritter, M., Jiao, C., Midgley, P., Clegg, W., 2011. Three-dimensional electron backscattered diffraction analysis of deformation in MgO micropillars. Acta Mater. 59, 7241–7254.

Kubin, L., Devincre, B., Tang, M., 1998. Mesoscopic modelling and simulation of plasticity in FCC and BCC crystals: dislocation intersections and mobility. J. Comput. Aided Mater. Des. 5, 31–54.

Kubin, L., Madec, R., Devincre, B., 2003. Dislocation intersections and reactions in FCC and BCC crystals. In: Zbib, H., Lassila, D., Levine, L., Hemker, K. (Eds.), Multiscale Phenomena in Materials Experiments and Modeling Related to Mechanical Behavior. Materials Research Society Symposium Proceedings, Warrendale, PA, pp. 25–36.

Madec, R., 2001. Des intersections entre dislocations à la plasticité du monocristal CFC: Etude par dynamique des dislocations (Ph.D. thesis). University of Paris XI.

Madec, R., Devincre, B., Kubin, L., 2002a. On the nature of attractive dislocation crossed states. Comput. Mater. Sci. 23, 219–224.

Madec, R., Devincre, B., Kubin, L., 2002b. From dislocation junctions to forest hardening. Phys. Rev. Lett. 89, 2555081–2555084.

Madec, R., Devincre, B., Kubin, L., Argaman, N., Levy, O., Makov, G., 2004. On the use of periodic boundary conditions in dislocation dynamics simulations. In: IUTAM Symposium on Mesoscopic Dynamics of Fracture Process and Materials Strength. Proceedings of the IUTAM

Symposium, Osaka, Japan, pp. 35–45, 6-11 July, 2003, Volume in celebration of Professor Kitagawa's retirement.
Madec, R., Devincre, B., Kubin, L., Hoc, T., Rodney, D., 2003. The role of collinear interaction in dislocation-induced hardening. Science 301, 1879–1882.
Madec, R., Kubin, L., 2004. Dislocations interactions and symmetries in BCC crystals. In: IUTAM Symposium on Mesoscopic Dynamics of Fracture Process and Materials Strength. Proceedings of the IUTAM symposium, Osaka, Japan, pp. 69–79, 6-11 July, 2003, Volume in celebration of Professor Kitagawa's retirement.
Mecking, H., Kocks, U., 1981. Kinetics of flow and strain-hardening. Acta Metall. 29, 1865–1875.
Merkel, S., Wenk, H., Shu, J., Shen, G., Gillet, P., Mao, H., Hemley, R., 2002. Deformation of polycrystalline MgO at pressures of the lower mantle. J. Geophys. Res. 107, 2271–2288.
Messerschmidt, U., 2010. Dislocation Dynamics During Plastic Deformation. Springer, Berlin.
Monnet, G., Devincre, B., Kubin, L., 2004. Dislocation study of prismatic slip systems and their interactions in hexagonal close packed metals: application to zirconium. Acta Mater. 52, 4317–4328.
Queyreau, S., 2008. Etude des mécanismes d'écrouissage sous irradiation de la ferrite par simulations de Dynamique des Dislocations (Ph.D. thesis). University of Paris Pierre et Marie Curie.
Robinson, W., 1972. Amplitude-independent mechanical damping in alkali halides. J. Mater. Sci. 7, 115–123.
Routbort, J., 1979. Work hardening and creep of MgO. Acta Metall. 27, 649–661.
Saada, G., 1960. Sur le durcissement dû à la recombinaison des dislocations. Acta Metall. 8, 841–847.
Sato, F., Sumino, K., 1980. The yield strength and dynamic behaviour of dislocations in MgO crystals at high temperatures. J. Mater. Sci. 15, 1625–1634.
Singh, R., Singh, M., Singh, R., 2008. Acoustical dissipation due to phonon-phonon interaction, thermoelastic loss and dislocation damping in MnO and CoO. J. Acoust. Soc. Am. 123, 3359–3364.
Srinivasan, M., Stoebe, T., 1974. Temperature dependence of yielding and work-hardening rates in magnesium oxide single crystals. J. Mater. Sci. 9, 121–128.
Takeuchi, S., Koizumi, H., Suzuki, T., 2009. Peierls stress and kink pair energy in NaCl type crystals. Mater. Sci. Eng. A 521, 90–93.
Washburn, J., Groves, G., Kelly, A., Williamson, G., 1960. Electron microscope observations of deformed magnesium oxide. Philos. Mag. 5, 991–999.
Wickham, L., Schwarz, K., Stölken, J., 1999. Rules for forest interactions between dislocations. Phys. Rev. Lett. 83, 4574–4577.